Cancer Cell
Article

Hotspot Mutations in *H3F3A* and *IDH1* Define Distinct Epigenetic and Biological Subgroups of Glioblastoma

Dominik Sturm,[1,42] Hendrik Witt,[1,7,42] Volker Hovestadt,[2,42] Dong-Anh Khuong-Quang,[11,42] David T.W. Jones,[1] Carolin Konermann,[3] Elke Pfaff,[1] Martje Tönjes,[2] Martin Sill,[4] Sebastian Bender,[1] Marcel Kool,[1] Marc Zapatka,[2] Natalia Becker,[4] Manuela Zucknick,[4] Thomas Hielscher,[4] Xiao-Yang Liu,[11] Adam M. Fontebasso,[12] Marina Ryzhova,[13] Steffen Albrecht,[14] Karine Jacob,[11] Marietta Wolter,[15] Martin Ebinger,[16] Martin U. Schuhmann,[17] Timothy van Meter,[18] Michael C. Frühwald,[19] Holger Hauch,[20] Arnulf Pekrun,[21] Bernhard Radlwimmer,[2] Tim Niehues,[22] Gregor von Komorowski,[23] Matthias Dürken,[23] Andreas E. Kulozik,[7] Jenny Madden,[24] Andrew Donson,[24] Nicholas K. Foreman,[24] Rachid Drissi,[25] Maryam Fouladi,[25] Wolfram Scheurlen,[26] Andreas von Deimling,[5,9] Camelia Monoranu,[27] Wolfgang Roggendorf,[27] Christel Herold-Mende,[8] Andreas Unterberg,[8] Christof M. Kramm,[28] Jörg Felsberg,[15] Christian Hartmann,[29] Benedikt Wiestler,[10] Wolfgang Wick,[10] Till Milde,[6,7] Olaf Witt,[6,7] Anders M. Lindroth,[3] Jeremy Schwartzentruber,[30] Damien Faury,[11] Adam Fleming,[11] Magdalena Zakrzewska,[31] Pawel P. Liberski,[31] Krzysztof Zakrzewski,[32] Peter Hauser,[33] Miklos Garami,[33] Almos Klekner,[34] Laszlo Bognar,[34] Sorana Morrissy,[35] Florence Cavalli,[35] Michael D. Taylor,[35] Peter van Sluis,[36] Jan Koster,[36] Rogier Versteeg,[36] Richard Volckmann,[36] Tom Mikkelsen,[37] Kenneth Aldape,[38] Guido Reifenberger,[15] V. Peter Collins,[39] Jacek Majewski,[40] Andrey Korshunov,[5] Peter Lichter,[2] Christoph Plass,[3,41,*] Nada Jabado,[11,41,*] and Stefan M. Pfister[1,7,41,*]

[1]Division of Pediatric Neurooncology
[2]Division of Molecular Genetics
[3]Division of Epigenetics and Cancer Risk Factors
[4]Division of Biostatistics
[5]Clinical Cooperation Unit Neuropathology
[6]Clinical Cooperation Unit Pediatric Oncology
German Cancer Research Center (DKFZ) Heidelberg, 69120 Heidelberg, Germany
[7]Department of Pediatric Oncology, Hematology, and Immunology
[8]Department of Neurosurgery
[9]Department of Neuropathology
[10]Department of Neurooncology
Heidelberg University Hospital, 69120 Heidelberg, Germany
[11]Departments of Pediatrics and Human Genetics, McGill University
[12]Division of Experimental Medicine, Montreal Children's Hospital
McGill University Health Center Research Institute, Montreal, QC H3Z 2Z3, Canada
[13]NN Burdenko Neurosurgical Institute, Moscow, 125047, Russia
[14]Department of Pathology, Montreal Children's Hospital, McGill University Health Center Research Institute, Montreal, QC H3H 1P3, Canada
[15]Department of Neuropathology, Heinrich-Heine-University, 40225 Düsseldorf, Germany
[16]Department of Hematology and Oncology, Children's University Hospital Tübingen, 72076 Tübingen, Germany
[17]Department of Neurosurgery, University Hospital Tübingen, 76076 Tübingen, Germany
[18]Virginia Commonwealth University, Richmond, VA 23298, USA
[19]Pediatric Hospital, Klinikum Augsburg, 86156 Augsburg, Germany
[20]Pediatric Hospital, Klinikum Heilbronn, 74078 Heilbronn, Germany
[21]Prof.-Hess-Kinderklinik, Klinikum Bremen-Mitte, 28177 Bremen, Germany
[22]Children's Hospital, Helios Clinics, 47805 Krefeld, Germany
[23]Children's University Hospital, 68135 Mannheim, Germany
[24]Department of Pediatrics, University of Colorado Denver, Aurora, CO 80045, USA
[25]Division of Oncology, Cincinnati Children's Hospital Medical Center, Cincinnati, OH 45229, USA
[26]Cnopf'sche Kinderklinik, Nürnberg Children's Hospital, 90419 Nürnberg, Germany
[27]Department of Neuropathology, Institute of Pathology, University Würzburg, 97080 Würzburg, Germany
[28]University Children's Hospital, Martin Luther University Halle-Wittenberg, 06120 Halle, Germany
[29]Institute of Pathology, Department of Neuropathology, Hannover Medical School, 30175 Hannover, Germany
[30]McGill University and Genome Quebec Innovation Centre, Montreal, QC H3A 1A4, Canada
[31]Department of Molecular Pathology and Neuropathology, Medical University of Lodz 92-216 Poland
[32]Department of Neurosurgery, Polish Mother's Memorial Hospital Research Institute, Lodz 93-338 Poland
[33]2nd Department of Paediatrics, Semmelweis University, Budapest H-1094 Hungary
[34]Department of Neurosurgery, Medical and Health Science Center, University of Debrecen, H-4032 Debrecen, Hungary
[35]Program in Developmental and Stem Cell Biology, Division of Neurosurgery, Arthur and Sonia Labatt Brain Tumour Research Centre, Hospital for Sick Children, University of Toronto, Toronto, ON M4N 1X8, Canada
[36]Department of Oncogenomics, AMC, University of Amsterdam, Amsterdam 1105 AZ, The Netherlands
[37]Departments of Neurology and Neurosurgery, Henry Ford Hospital, Detroit, MI 48202, USA
[38]Department of Neuro-Oncology, University of Texas MD Anderson Cancer Center, Houston, TX 77030, USA
[39]Division of Molecular Histopathology, Department of Pathology, University of Cambridge, Cambridge, CB2 0QQ, United Kingdom

[40]Department of Human Genetics, McGill University, Montreal, QC H3Z 2Z3, Canada
[41]These authors contributed equally to this work
[42]These authors contributed equally to this work
*Correspondence: c.plass@dkfz.de (C.P.), nada.jabado@mcgill.ca (N.J.), s.pfister@dkfz.de (S.M.P.)
http://dx.doi.org/10.1016/j.ccr.2012.08.024

SUMMARY

Glioblastoma (GBM) is a brain tumor that carries a dismal prognosis and displays considerable heterogeneity. We have recently identified recurrent *H3F3A* mutations affecting two critical amino acids (K27 and G34) of histone H3.3 in one-third of pediatric GBM. Here, we show that each *H3F3A* mutation defines an epigenetic subgroup of GBM with a distinct global methylation pattern, and that they are mutually exclusive with *IDH1* mutations, which characterize a third mutation-defined subgroup. Three further epigenetic subgroups were enriched for hallmark genetic events of adult GBM and/or established transcriptomic signatures. We also demonstrate that the two *H3F3A* mutations give rise to GBMs in separate anatomic compartments, with differential regulation of transcription factors *OLIG1*, *OLIG2,* and *FOXG1*, possibly reflecting different cellular origins.

INTRODUCTION

Glioblastoma (GBM; World Health Organization [WHO] grade IV), the most common primary brain tumor, carries a universally dismal prognosis in children and adults (Louis et al., 2007). With evidence emerging recently of age-specific molecular and genetic differences, it is now becoming apparent that pediatric GBM is largely biologically distinct from adult GBM. Based on similarities in recurrent genomic aberrations (Bax et al., 2010; McLendon et al., 2008; Paugh et al., 2010; Qu et al., 2010; Schiffman et al., 2010; Zarghooni et al., 2010), it was long thought that pediatric GBMs more closely resembled adult "secondary" GBM, which arise from a preceding lower-grade lesion. However, stepwise transformation from less-malignant gliomas into GBM rarely occurs in children (Broniscer et al., 2007). Furthermore, *IDH1* or *IDH2* mutations, which are found in up to 98% of adult secondary GBM, are very rare in childhood GBM (<10%) (Antonelli et al., 2010; Balss et al., 2008; De Carli et al., 2009; Paugh et al., 2010; Pollack et al., 2011; Schiffman et al., 2010; Setty et al., 2010; Yan et al., 2009).

We recently identified two recurrent somatic mutations in the *H3F3A* gene, affecting highly conserved residues of its encoded protein, the replication-independent histone 3 variant H3.3, in one-third of pediatric GBMs (Schwartzentruber et al., 2012). Mutations in a protein complex comprised of H3.3 and ATRX/DAXX were detected in 45% of cases, and were shown to be associated with *TP53* mutations and alternative lengthening of telomeres (ALT). The H3.3 mutations result in amino acid substitutions at K27 or G34—at or near residues targeted by key post-translational modifications that regulate H3.3's activity in governing gene expression (Hyland et al., 2011)—and were shown to be linked to distinct transcriptional profiles (Schwartzentruber et al., 2012). Methylation of K27 and K36 is also disrupted by elevated levels of the onco-metabolite 2-hydroxyglutarate (2-HG) resulting from gain-of-function mutations in *IDH1* (Chowdhury et al., 2011; Xu et al., 2011), which was previously shown to be associated with a distinct Glioma-CpG-Island Methylator Phenotype (G-CIMP) (Noushmehr et al., 2010).

In the present study, we further investigate the heterogeneity of glioblastoma across the entire age spectrum, and elucidate the impact of *H3F3A* mutations on the GBM epigenome.

RESULTS

Integrated Molecular Classification of Glioblastoma

We used an integrative approach based on epigenetic, copy-number, expression, and genetic analyses to investigate the heterogeneity of glioblastoma across all age groups. An overview of all GBM samples subjected to various analyses is given in Figure S1A available online.

Significance

GBM is the most common and also the most devastating brain tumor, with a 5-year survival rate below 10%. We present strong evidence that GBM can be subclassified into multiple groups, indistinguishable by histological appearance, but correlating with molecular-genetic factors as well as key clinical variables such as patient age and tumor location. We identified six epigenetic GBM subgroups displaying characteristic global DNA methylation patterns, harboring distinct hotspot mutations, DNA copy-number alterations, and transcriptomic patterns. These findings may guide the identification of innovative subgroup-specific treatments, e.g., targeted epigenetic therapies for H3.3-mutated variants, and improve the design of future clinical trials. Our study enables classification of GBM across the entire age continuum into biologically meaningful subgroups carrying clinical implications.

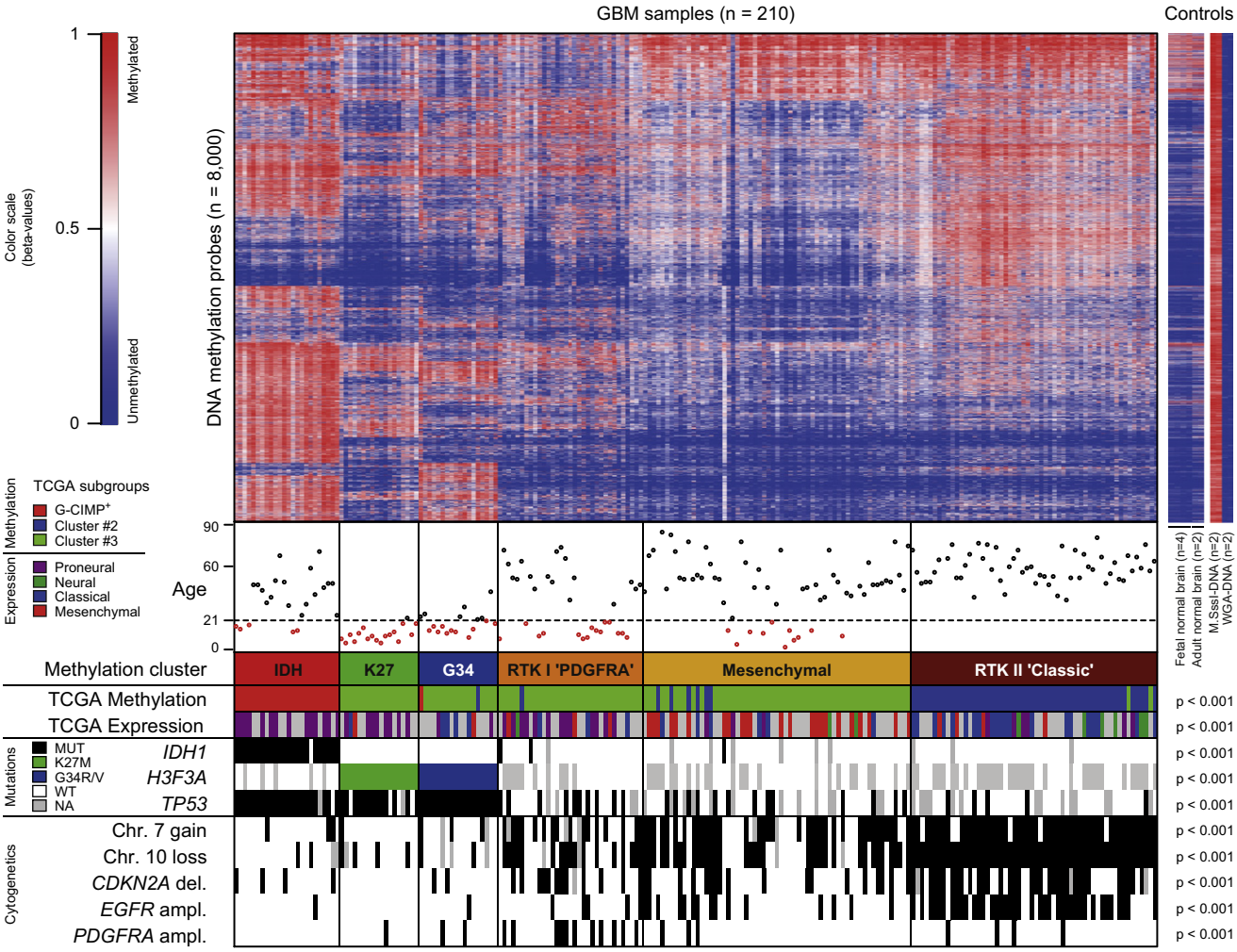

Figure 1. Methylation Profiling Reveals the Existence of Six Epigenetic GBM Subgroups

Heatmap of methylation levels in six GBM subgroups identified by unsupervised k-means consensus clustering, and control samples as indicated. Each row represents a probe; each column represents a sample. The level of DNA methylation (beta-value) is represented with a color scale as depicted. For each sample (n = 210), patient age, subgroup association, mutational status, and cytogenetic aberrations are indicated.

See also Figure S1 and Tables S1 and S2.

We investigated a cohort of GBMs from children (n = 59) and adult patients (n = 77) for genome-wide DNA methylation patterns using the Illumina 450k methylation array, and complemented our data with unpublished profiles of 74 adult GBM samples generated by The Cancer Genome Atlas (TCGA) Consortium (McLendon et al., 2008) (Table S1). Consensus clustering using the 8,000 most variant probes across the data set robustly identified six distinct DNA methylation clusters (Figures 1 and S1B). Based on correlations with mutational status, DNA copy-number aberrations, and gene expression signatures, as outlined below, we have labeled these subgroups "IDH," "K27," "G34," "RTK I (PDGFRA)," "Mesenchymal," and "RTK II (Classic)."

A striking finding of this integrated analysis is that *H3F3A* K27 and G34 mutations were exclusively distributed to the K27 (18/18) and G34 (18/18) clusters, respectively ($p < 0.001$; Fisher's exact test) (Figure 1). The IDH group contained 88% of *IDH1*-mutated tumors (23/26) ($p < 0.001$) and displayed concerted, global hypermethylation (Figures 1, 2A, and 2B), thereby expanding the previously described link between *IDH1* mutation and G-CIMP$^+$ tumors to a pediatric setting (Noushmehr et al., 2010). In contrast, tumors in the G34 cluster specifically showed widespread hypomethylation across the whole genome, and especially in nonpromoter regions, when compared with all other subgroups (Figures 2A and 2B). This suggests the existence of a more global version of a CpG hypomethylator phenotype (CHOP), as proposed for a small number of genes in gastric cancer (Kaneda et al., 2002). More detailed mapping of differentially methylated regions revealed that the hypomethylation observed in *H3F3A* G34-mutated tumors was particularly prominent at chromosome ends (Figures 2C and 2D), potentially linking subtelomeric demethylation to alternative lengthening of telomeres, which is most frequently observed in this subgroup (Schwartzentruber et al., 2012).

Of note, all mutations in *H3F3A* and *IDH1* were mutually exclusive ($p < 0.001$) (Figure 1). To further test this observation, we

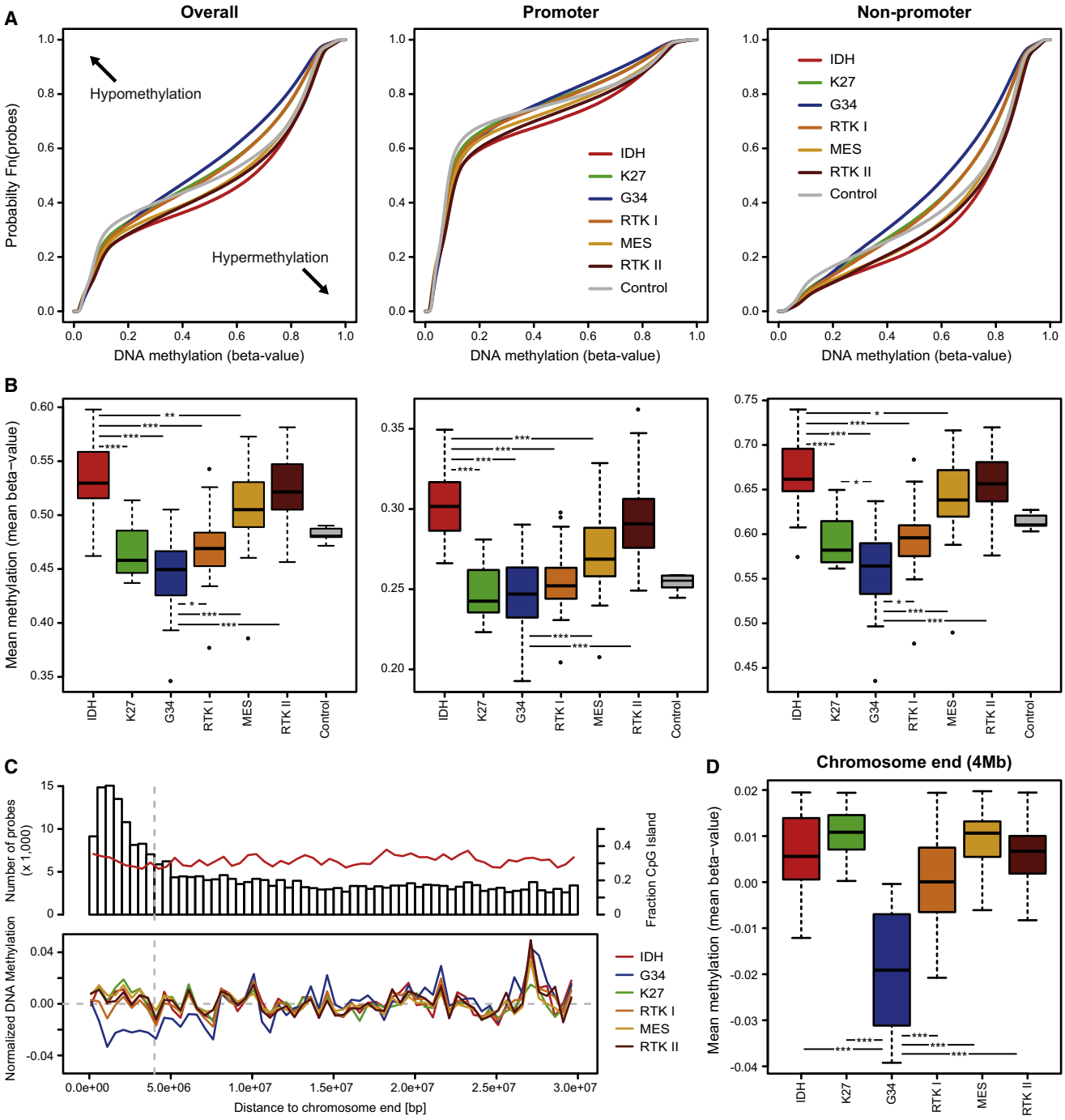

Figure 2. Global DNA Methylation Patterns in GBM Subgroups

(A) Distinct patterns of global DNA methylation in GBM subgroups as identified by consensus clustering. The empirical cumulative distribution function for DNA methylation levels (beta-values) is plotted individually for each subgroup.

(B) Overall DNA methylation levels (mean beta-values) of individual GBM methylation subgroups. Significant differences (***$p < 0.001$; **$p < 0.01$; *$p < 0.05$) to IDH and G34 subgroups are indicated.

(C) Upper panel: Probe density in respect of distance to chromosome end. The fraction of probes located within CpG-Islands (red line) remains stable. Lower panel: Mean methylation value per subgroup within windows of 500kb, normalized to control samples. Individual samples are normalized by the mean overall methylation value.

(D) Mean methylation value within 4 Mb to the chromosome end normalized to the mean overall methylation value and to control samples. Significant differences (***$p < 0.001$) between subgroups compared to G34 tumors are indicated. MES, Mesenchymal.

See also Figure S2.

extended the targeted sequencing analysis of *H3F3A* and *IDH1* to include 460 GBM samples from patients covering a broad age range (Figure S1C; Table S2). Even in this expanded series, no co-occurring mutations in *H3F3A* and *IDH1* were detected ($p < 0.001$), and the age distribution confirmed reported associations of certain mutations with GBM in children (*H3F3A* K27), adolescent patients (*H3F3A* G34), and young adult patients (*IDH1*) (Khuong-Quang et al., 2012; Schwartzentruber et al., 2012; Yan et al., 2009) (Figure S1C; Table S2). As we have shown, *TP53* mutations largely overlap with *H3F3A* mutations in pediatric GBM (Schwartzentruber et al., 2012), similar to the association of *TP53* and *IDH1* mutations in adults (Yan et al., 2009). This observation also holds true in our larger cohort, with a high enrichment of *TP53* mutations in the G34 (18/18), IDH (22/24), and K27 (13/18) clusters ($p < 0.001$) (Figure 1).

Since pediatric GBMs have been shown to display a distinct spectrum of focal copy-number aberrations (CNAs) compared with their adult counterparts (Bax et al., 2010; Paugh et al., 2010; Qu et al., 2010), we integrated DNA methylation clusters with copy-number data derived from the methylation arrays (Figures 1 and S1D). Interestingly, *PDGFRA* amplification was significantly more common in the RTK I "PDGFRA" cluster than any other subgroup (11/33; $p < 0.001$), hence our proposed name for this group. The RTK II "Classic" cluster demonstrated a very high frequency of whole chromosome 7 gain (50/56; $p < 0.001$) and whole chromosome 10 loss (56/56; $p < 0.001$), as well as frequent homozygous deletion of *CDKN2A* (35/56; $p < 0.001$) and amplification of *EGFR* (39/56; $p < 0.001$) (Figures 1 and S1D)—all hallmark CNAs of adult GBM (Louis et al., 2007), as reflected by the complete absence of pediatric patients in this cluster. Overall, tumors from the IDH, K27, and G34 clusters were mostly devoid of the detected CNAs associated with the other GBM subgroups (amplifications of *PDGFRA* and *EGFR*, deletion of *CDKN2A*, chromosome 7 gain, and chromosome 10 loss) (Figure 1; Table S1), in keeping with a previously reported finding in G-CIMP$^+$ tumors (Noushmehr et al., 2010).

To additionally place the methylation subgroups proposed here into the context of previous GBM classification systems, we used the gene expression signature described by the TCGA to classify 122 of the above tumors with available transcriptome data into one of four gene expression subtypes: Proneural, Neural, Mesenchymal, and Classical (Verhaak et al., 2010) (Figure 1; Table S1). This further confirmed the prototypic nature of tumors in the RTK II "Classic" cluster, which was clearly enriched for "Classical" expression profiles ($p < 0.001$). The RTK I "PDGFRA" cluster was highly enriched for "Proneural" expression ($p = 0.01$), further substantiating the previously reported association of *PDGFRA* amplification with this expression subtype (Verhaak et al., 2010). As expected, all tumors in the IDH cluster displayed "Proneural" expression patterns. Interestingly, the K27 cluster also showed a clear enrichment of tumors with a "Proneural" signature ($p < 0.01$), indicating that this expression subtype can be divided into subgroups harboring distinct genomic aberrations based on methylation profiling and targeted gene sequencing. "Mesenchymal" gene expression was mostly restricted to one methylation subgroup ($p < 0.001$), that showed a much lower incidence of typical GBM-related CNAs, generally fewer copy-number changes, and no characteristic point mutations. We therefore termed this methylation cluster, which displayed the largest similarity with normal brain methylation patterns, "Mesenchymal." Copy-number aberrations in these samples were, however, observed at a similar amplitude as in other cases, indicating an absence of excess stromal contamination.

Our finding of six GBM methylation clusters is different from a TCGA study using Illumina 27k arrays, which identified three methylation clusters in an adult GBM cohort (Noushmehr et al., 2010). Applying their signature to our data set, however, showed that two clusters (G-CIMP$^+$ and Cluster #3) mapped almost exactly to two of our subgroups (IDH and RTK II "Classic,", respectively, $p < 0.001$) (Figure 1). By adding pediatric cases to the study cohort, we demonstrate that TCGA methylation Cluster #2 can be further divided into four biologically distinct subgroups, defined by a clear enrichment for mutations (K27, G34), CNAs (PDGFRA), and/or gene expression signatures (Mesenchymal). The same DNA methylation clusters were apparent when restricting our analyses to the pediatric population, with the exception of the RTK II "Classic" cluster, which is not represented in the pediatric population (Figure S1E). Notably, by analyzing tumors from patients spanning a broad age spectrum, we further observed a clear age-dependent increase in overall DNA methylation levels (Figure S2A), even after adjusting our analysis to exclude tumors with age-related mutations in *IDH1* or *H3F3A* (Figure S2B).

GBM Subgroups Show Correlations with Clinicopathological Variables

The DNA methylation clusters described here were closely associated with specific age groups, pointing toward the biological diversity of epigenetic GBM subgroups (Figure 1). While the K27 cluster predominantly consisted of childhood patients (median age 10.5 years, range 5–23 years), patients in the G34 cluster were found mostly around the threshold between the adolescent and adult populations (median age 18 years, range 9–42 years), as previously suggested (Schwartzentruber et al., 2012). The RTK I "PDGFRA" cluster also harbored a proportion of pediatric patients (median age 36 years, range 8–74 years), in line with reports of *PDGFRA* CNAs being more prevalent in childhood high-grade gliomas (Bax et al., 2010; Paugh et al., 2010; Qu et al., 2010). The Mesenchymal cluster displayed a widespread age distribution (median age 47, range 2–85 years). The IDH and RTK II "Classic" clusters were mostly comprised of younger adult (median age 40 years, range 13–71 years) and older adult (median age 58, range 36–81 years) patients, respectively, reflecting the established differences in patient age between *IDH1*-mutated/G-CIMP$^+$ and *IDH1* WT adult GBM (Noushmehr et al., 2010; Yan et al., 2009).

The epigenetic GBM subgroups identified here also showed mutation-specific patterns of tumor location in the central nervous system (Figure 3A). While K27-mutated tumors were predominantly seen in midline locations, e.g., thalamus, pons, and the spinal cord (21/25 cases with available data), tumors from all other subgroups almost exclusively arose in the cerebral hemispheres (86/92, $p < 0.001$). To further investigate this association of mutation type and location, we investigated the transcriptomic profiles of *H3F3A*-mutated samples ($n = 13$). Gene signatures characteristic for K27 and G34 mutant GBMs were

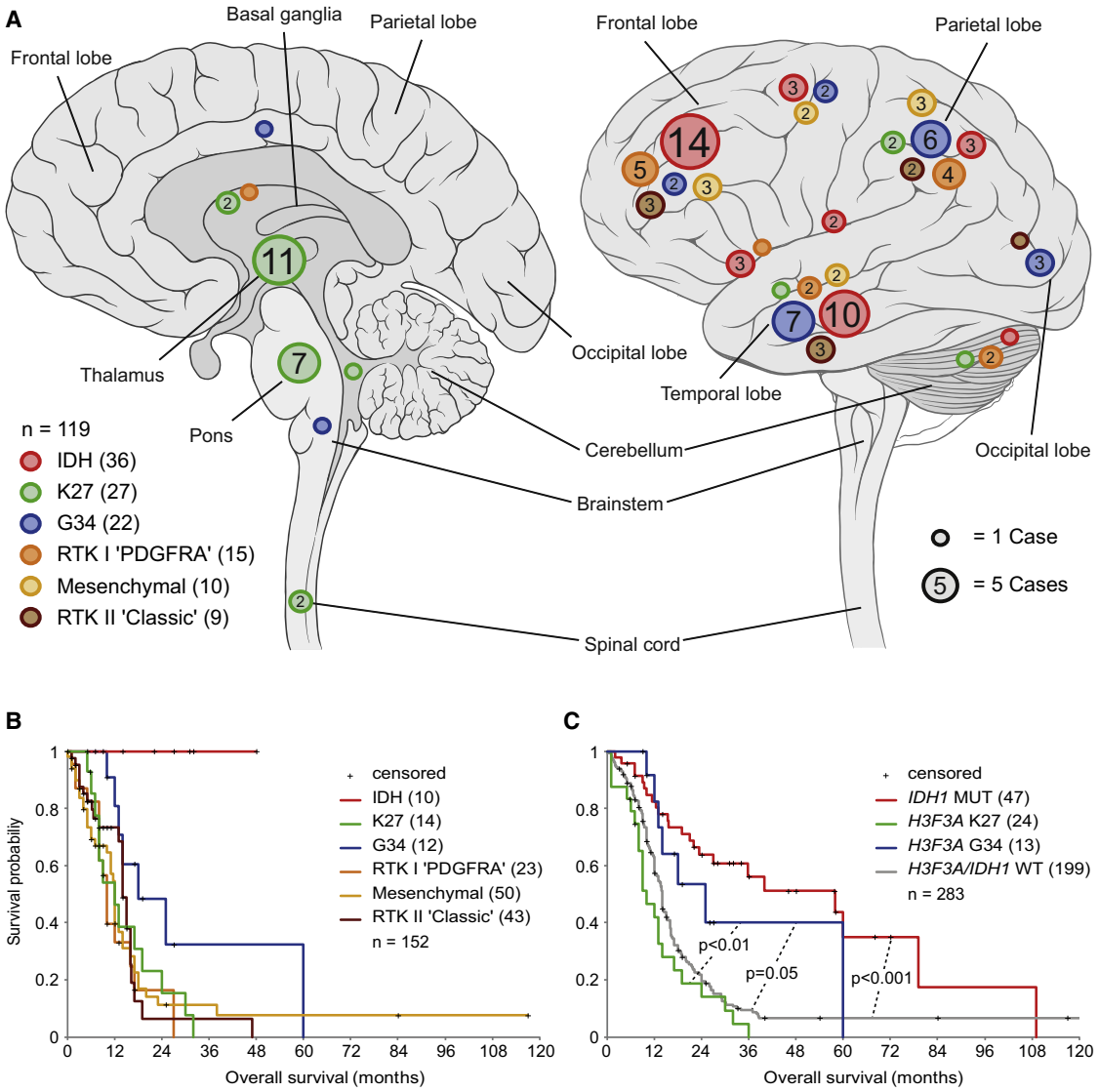

Figure 3. Epigenetic Subgroups of GBM Correlate with Distinct Clinical Characteristics

(A) Location of 119 GBMs in the human central nervous system grouped by methylation clusters. The number of cases in each group is indicated within the circles. Circles without numbers represent single cases. Different colors indicate methylation cluster affiliation. Tumors occurring in midline locations are depicted in the sagittal view (left panel), tumors occurring in the cerebral and cerebellar hemispheres are depicted in the exterior view (right panel).

(B and C) Kaplan-Meier survival curves for GBM subgroups defined by methylation profiling (B), and mutation analysis (C). The p values were computed by log rank tests between subgroups.

See also Figure S3.

applied to a published series of 1,340 transcriptomic profiles representing multiple regions of the developing and adult human brain (Kang et al., 2011; Figure S3). The G34 mutant signature appeared to be most strongly expressed in early embryonic regions and early- to mid-fetal stages of neocortex and striatum development. In contrast, the K27 signature most closely matched with mid- to late-fetal stages of striatum and thalamus development. Thus, G34 and K27 mutant GBMs seem to show expression patterns of early developmental stages correlating with their subsequent tumor location, possibly indicating different cellular origins and/or time of tumor initiation for these two subgroups.

Correlating our proposed methylation clusters with patient survival indicated differences between mutation-defined subgroups, but this was somewhat restricted by the low number of patients with available survival data in each subgroup (Figure 3B). We therefore enlarged our survival analysis to include all tumors with known *H3F3A* and *IDH1* mutation status (Figure 3C). As expected, patients with *IDH1* mutant tumors had a significantly longer overall survival (OS) than patients with *H3F3A* and *IDH1* WT tumors ($p < 0.001$) (Noushmehr et al., 2010; Parsons et al., 2008; Yan et al., 2009). Notably, G34 mutant GBM patients also showed a trend toward a better OS than WT tumor patients, with marginal statistical significance ($p = 0.05$). In

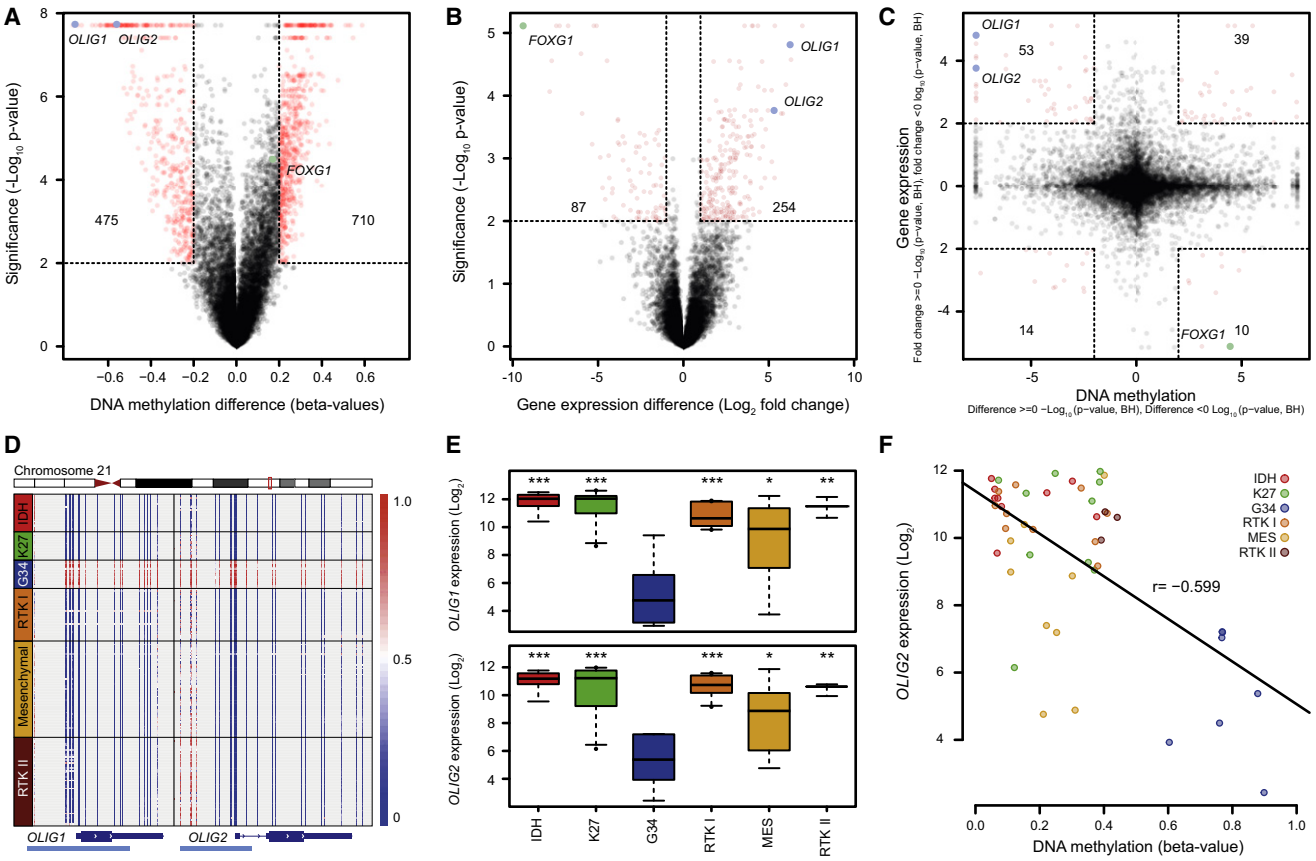

Figure 4. Identification of Marker Genes Affected by Differential Methylation and Expression in GBM Subgroups

(A and B) Volcano plots illustrating differences in DNA methylation (A) and gene expression (B) between tumors from the K27 and G34 subgroups. Difference in beta-values (A) and Log_2 fold change in gene expression values (B) are plotted on the x axis, adjusted p values calculated using the SAM method are plotted on the y axis.

(C) Starburst plot integrating DNA methylation (x axis) and gene expression (y axis) data.

(D) Methylation levels at the *OLIG1* and *OLIG2* loci across all 210 GBM samples investigated. Each row represents one sample; each vertical bar represents one CpG-site. Light blue bars indicate promoter regions. Methylation levels are represented by a color scale as indicated.

(E) Mean gene expression levels of *OLIG1* (upper panel) and *OLIG2* (lower panel) across GBM subgroups (n = 48). Significant differences (***$p < 0.001$; **$p < 0.01$; *$p < 0.05$) between subgroups compared to G34 tumors are indicated.

(F) Inverse correlation of promoter methylation (x axis) and gene expression (y axis) of *OLIG2* across GBM methylation subgroups (n = 48; Pearson's correlation coefficient, *r*). MES, Mesenchymal.

See also Figure S4 and Table S3.

contrast, patients with K27 mutations tended toward an even shorter OS than patients with WT tumors, although this did not reach statistical significance ($p = 0.12$). Comparing the two *H3F3A* mutations, patients harboring G34-mutated tumors clearly had a longer OS than patients with tumors carrying the K27 mutation ($p < 0.01$). While this association may be partly linked to G34-mutated tumors being more accessible to surgery than the midline K27-mutated tumors, the better prognosis of G34 versus K27 was independent of location for those cases where both mutation type and tumor site information were available ($p = 0.02$; HR = 0.20, 95% CI = 0.05–0.77; Cox proportional hazards model).

Integrating Methylome and Transcriptome Data Identifies Marker Genes of GBM Subgroups

A combined analysis of DNA methylation and gene expression data was used to identify subgroup-specific differentially regulated genes (Figures 4A–4C and S4A–4C; Table S3). This analysis revealed Oligodendrocyte Lineage Genes 1 and 2 (*OLIG1* and *OLIG2*) and the neural development gene *FOXG1* as top candidates for further analysis in *H3F3A*-mutated GBMs (Figure 4A–4C). DNA hypermethylation across the *OLIG1* and *OLIG2* loci occurred exclusively in G34-mutated tumors, which concurrently displayed significantly lower *OLIG1* and *OLIG2* gene expression (Figure 4D–4F). Interestingly, this pattern closely mimics that of embryonic stem cells, where epigenetic inactivation of OLIG1 and OLIG2 has been proposed as a mechanism to prevent neural lineage commitment (Meissner et al., 2008). Expression of *FOXG1* was significantly lower in K27-mutated tumors than in all other subgroups, accompanied by higher levels of promoter methylation (Figures S4A, S4D, and S4E). This comparative analysis also further supported our suggestion of a CHOP-like phenotype in G34 tumors, as most of the differentially methylated genes were found to be

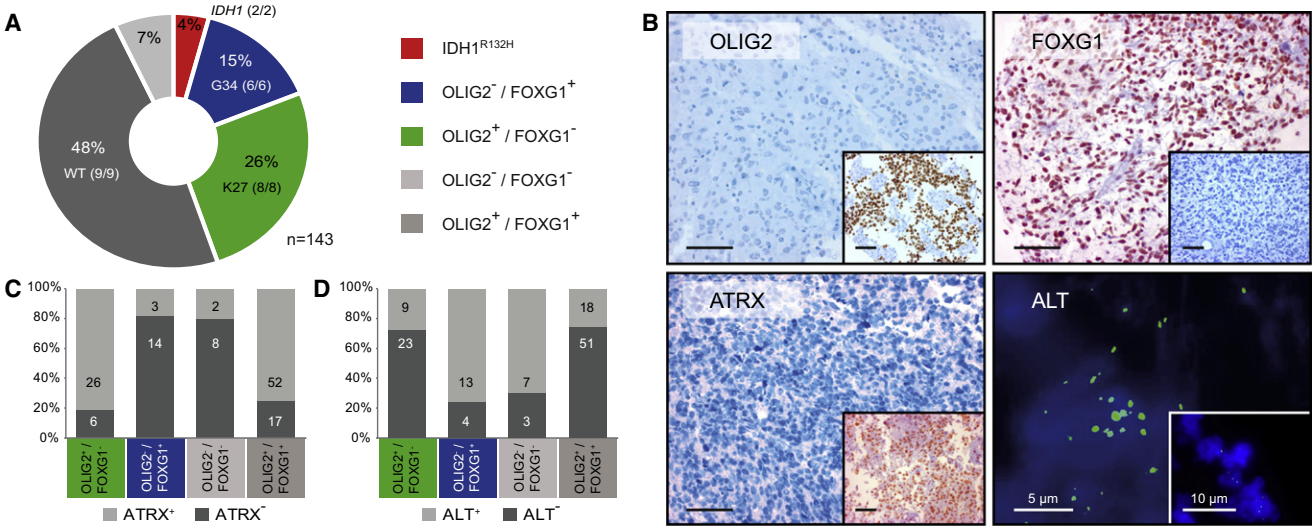

Figure 5. Identification of *H3F3A*-Mutated GBMs by Differential Protein Expression Patterns

(A) Classification of 143 pediatric GBMs according to protein expression of OLIG2, FOXG1, and mutated IDH1 ($IDH1^{R132H}$). Numbers in brackets indicate samples with known *H3F3A* and *IDH1* mutation status as predicted by immunohistochemistry and verified by targeted gene sequencing, respectively.

(B) Typical pattern of $OLIG2^{-}$/$FOXG1^{+}$ cells with concomitant loss of ATRX protein expression and ALT as observed in G34-mutated GBMs. Insets show contrasting staining results for comparison. Scale bars represent 100 µm unless indicated differently.

(C and D) Correlation of GBMs as classified in (A) with ATRX loss (C), and ALT (D).

See also Figure S5 and Table S4.

hypomethylated (1653/1946, 85%, Figure S4B) in this subgroup, in contrast to the hypermethylator G-CIMP pattern observed in the IDH subgroup (Figure S4C). Hypermethylation and concurrent downregulation of *TP73* antisense RNA 1 (*TP73-AS1*) was identified as a unique characteristic of this IDH/G-CIMP^{+} cluster (Figures S4D and S4F). Interestingly, inactivation of this gene by promoter methylation has been reported as a common mechanism in a high proportion of oligodendrogliomas, 80% of which are also known to harbor *IDH1* mutations (Pang et al., 2010).

Immunohistochemical Analysis Correctly Subclassifies Mutation-Defined GBM Subgroups

In an attempt to subgroup GBM samples based on differential protein expression—a method which is likely to be more suitable for possible clinical application—we used commercially available antibodies against OLIG2, FOXG1, and mutated IDH1 (R132H) to stain a tissue-microarray (TMA) with cores from 143 pediatric GBMs, and classified tumors according to their protein expression patterns (Figures 5A and 5B; Table S4). The resulting fractions of tumors with predicted mutations in *IDH1* ($IDH1^{R132H}$, n = 6) and *H3F3A* ($OLIG2^{+}$/$FOXG1^{-}$ for K27, n = 37, and $OLIG2^{-}$/$FOXG1^{+}$ for G34, n = 21) were consistent with the frequency of each mutation in the pediatric population as detected by targeted gene sequencing (Figure S1C). Our approach correctly classified GBMs with known *H3F3A* and *IDH1* mutation status, and revealed a frequent association between $OLIG2^{-}$/$FOXG1^{+}$ tumors (assumed to be G34-mutated), loss of ATRX protein expression, and an ALT phenotype (Figures 5B–D), as previously reported for *H3F3A* G34-mutated tumors (Schwartzentruber et al., 2012). The putative *H3F3A* mutant groups also did not overlap with tumors harboring IDH1 (R132H) mutations, and only one case with *EGFR* amplification and homozygous *CDKN2A* deletion was detected therein (Figure S5A). The correlation with clinicopathological variables, such as tumor location and patient survival, also reflected our findings from the array-based analysis (Figures S5B and S5C). Of note, rare tumors represented on the TMA occurring in the basal ganglia and the spinal cord were almost always found in the $OLIG2^{+}$/$FOXG1^{-}$ subgroup (and therefore predicted to harbor the *H3F3A* K27 mutation), further strengthening our hypothesis of the *H3F3A* K27 mutation as a unifying characteristic of midline GBM.

DISCUSSION

We have identified six biological subgroups of GBM based on global DNA methylation patterns, which correlate with specific molecular-genetic alterations and key clinical parameters. Our findings suggest that at least 30%–40% of pediatric/young adult GBMs are likely characterized by disrupted epigenetic regulatory mechanisms, associated with recurrent and mutually exclusive mutations in either *H3F3A* or *IDH1*, and aberrant DNA methylation patterns. Placing these subgroups into the context of previous molecular GBM classification schemes described by the TCGA (Noushmehr et al., 2010; Verhaak et al., 2010) revealed a clear correlation with DNA methylation clusters and a corresponding enrichment for previously established expression signatures in different epigenetic subgroups. We have also demonstrated that our proposed classification can refine that described by the TCGA for adult GBM, to give a stratification system that is applicable across all ages, and defines additional biologically meaningful subgroups. A simplified graphical summary of the key molecular and biological characteristics of the GBM subgroups as identified by our integrated classification strategy is given in Figure 6.

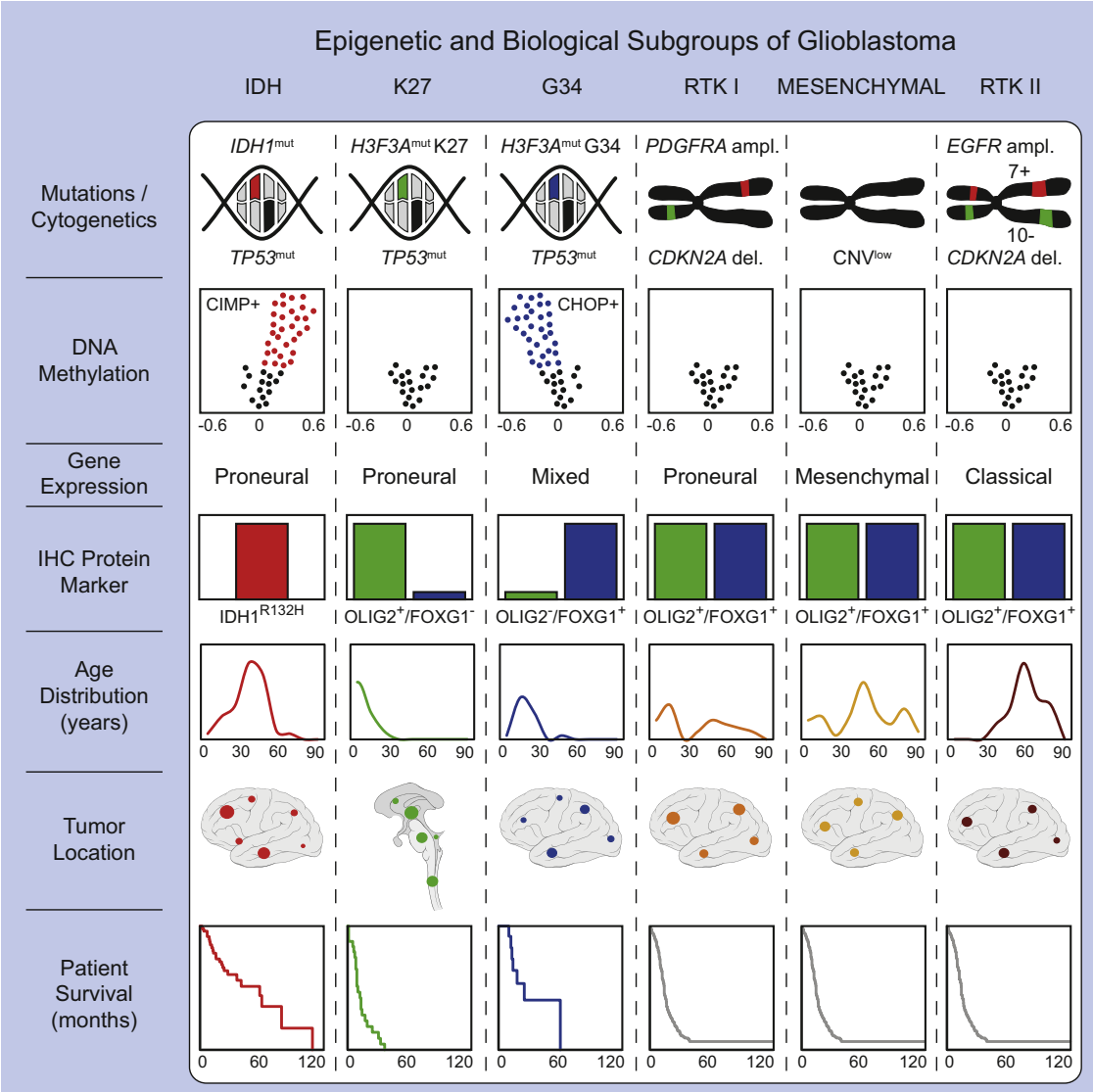

Figure 6. Graphical Summary of Key Molecular and Biological Characteristics of GBM Subgroups

Simplified schematic representation of key genetic and epigenetic findings in six GBM subgroups as identified by methylation profiling and correlations with clinical patient data.

We and others have recently described a high frequency of *H3F3A* K27 mutations in thalamic GBMs and in diffuse intrinsic pontine gliomas (DIPGs), suggesting that the latter likely represent an anatomically-defined subset of K27 mutant GBM (Khuong-Quang et al., 2012; Schwartzentruber et al., 2012; Wu et al., 2012). We now extend this observation to a larger subgroup of GBM, characterized by the K27M mutation, which almost exclusively occurs in midline locations, including rare tumors in the basal ganglia and the spinal cord. This is in line with a recent study by Puget et al. (2012) in which gene expression patterns of brainstem gliomas were found to resemble midline/thalamic tumors, indicating a closely related origin. The K27 subgroup also displays markedly lower expression of the ventral telencephalic marker *FOXG1* than other subgroups. Conversely, non-K27 tumors were restricted to hemispheric locations, further underlining the biological divergence of epigenetic GBM subgroups. While recurrent focal amplification of *PDGFRA* has been suggested as a key oncogenic event in pediatric DIPGs in some studies (Paugh et al., 2011; Puget et al., 2012; Zarghooni et al., 2010), midline-associated tumors in the K27 or OLIG2^{+}/FOXG1^{-} subgroups (including ten brainstem gliomas with known *PDGFRA* copy-number status) lacked this common feature in our series. *PDGFRA* amplification was, however, enriched in a subgroup of supratentorial hemispheric GBMs. In part, this discrepancy may be explained by the use of autopsy (and therefore post radio/chemotherapy) material in previous study cohorts of DIPGs, which might have been confounded by the higher incidence of *PDGFRA* amplifications observed in radiation-induced gliomas (Paugh et al., 2010). Nevertheless, amplifications of *PDGFRA* have also been

detected in small numbers of pretreatment samples (Paugh et al., 2011; Puget et al., 2012; Zarghooni et al., 2010), and post-treatment samples were not found to show increased widespread genomic instability (Paugh et al., 2011). This particularly clinically challenging subset of tumors clearly warrants further investigation, underlining the importance of routine stereotactic biopsy of DIPGs at the time of primary diagnosis.

OLIG2 has previously been reported as a universal marker for diffuse gliomas (Ligon et al., 2004), and OLIG2-positive progenitor-like cells of the subventricular zone have been suggested as potential glioma-initiating cells (Wang et al., 2009). There is also evidence that OLIG2-mediated modification of p53 function is required for complete inactivation of the latter in malignant gliomas, which typically show indirect loss of p53 activity through *MDM2* amplification or $p14^{ARF}$ deletion (Mehta et al., 2011). Here, we describe a distinct subgroup of GBM, harboring the *H3F3A* G34 mutation, in which OLIG1 and OLIG2 protein expression is absent. Given the ~100% mutation frequency of *TP53* in this subgroup, this may indicate a different pathogenesis of G34-mutated GBM, in which direct inactivation of p53 is required rather than via an OLIG2-dependent mechanism.

The previously reported association of *H3F3A* mutations, particular the G34 mutation, with loss of ATRX and ALT (Schwartzentruber et al., 2012) is further expanded upon here. Interestingly, the global CHOP that we observed in G34 mutants was particularly pronounced in subtelomeric regions, suggesting a possible mechanistic link with ALT in these tumors (Gonzalo et al., 2006). Whether this is a more general phenotype that can be observed in clinically and etiologically distinct subgroups of other human cancers, remains to be investigated.

The close link between *H3F3A* mutation type, tumor location, and differential expression of key neuronal lineage markers leads us to speculate that there may be differences in the cell of origin and/or the time of tumor development between these GBM subgroups. Although supported by the differential expression of mutant-specific gene signatures at different stages of human brain development, this remains to be formally shown. Also requiring further validation in larger, prospective cohorts is the association of the G34 mutation with better overall survival compared with *H3F3A* and *IDH1* WT tumors, and that of K27 mutation with potentially poorer prognosis, as observed in our series and a recent cohort of pediatric DIPGs (Khuong-Quang et al., 2012).

Given the location of the *H3F3A* mutations at or near critical regulatory histone residues, and their distinct methylation profiles, we consider it likely that the H3.3 mutations are directly involved in producing widespread aberrant DNA methylation and deregulation of gene expression. This has recently been shown for *IDH1* mutations, which alone are sufficient to induce the global epigenetic reprogramming of the G-CIMP phenotype in normal astrocytes (Turcan et al., 2012). Overproduction of the oncometabolite 2-hydroxyglutarate in *IDH1*-mutated cells inhibits the TET family of 5-methlycytosine hydroxylases and H3K27-specific demethylases. This is thought to lead to decreased 5-hydroxylmethycytosine and increased H3K27 methylation (Xu et al., 2011), resulting in aberrant DNA and histone methylation, and a block to differentiation (Christensen et al., 2011; Dang et al., 2009; Lu et al., 2012).

Seminal studies have shown that DNA methylation patterns are tightly linked to histone 3 lysine K27 trimethylation (H3K27me3) patterns (Brinkman et al., 2012; Statham et al., 2012), and in high-CpG-density promoters, loss of H3K4me3 and retention of H3K4me2 or H3K27me3 is correlated with an increase in DNA methylation (Meissner et al., 2008). Therefore, mutations affecting H3K27 methylation are likely to affect DNA methylation. In addition, mutations in ATRX have been shown to give rise to changes in the patterns of DNA methylation of several highly repeated sequences, which further supports the link between chromatin remodeling machinery and DNA methylation (Gibbons et al., 2000). Based on our current knowledge, the incorporation of H3.3 variants into the genome, and the subsequent effects on gene regulation, involve the H3.3 chaperone complex (including ATRX and DAXX) in a replication independent manner (Drané et al., 2010; Goldberg et al., 2010) but other factors also likely play a role. The exact mechanism by which the *H3F3A* mutations might be inducing epigenetic reprogramming requires further elucidation.

In conclusion, this study describes a number of findings that enhance our understanding of the heterogeneity of GBM, as well as shedding light on potential cellular origins and oncogenic pathways leading to gliomagenesis. We have identified potential prognostic biomarkers, which may be further exploited for molecular diagnostic purposes, and also provided a focus for future work at a basic and translational/targeted therapeutic level, particularly in a pediatric and young adult setting.

EXPERIMENTAL PROCEDURES

Patients and Tumor Samples

Primary tumor samples for methylation (n = 136; Table S1), mutation (n = 460; Table S2), and gene expression (n = 69) analysis and all clinical data were collected at the DKFZ (Heidelberg, Germany) and at McGill University (Montreal, Canada). Paraffin-embedded samples (n = 143; Table S4) for TMA analysis were collected from the Burdenko Neurosurgical Institute (Moscow, Russia) and from the Department of Neuropathology, University of Würzburg (Germany). Patient clinical details can be found in Table S1 for the methylation analysis data set and in Table S4 for the TMA cohort. All of the tumors were banked at the time of primary diagnosis between 1994 and 2011 in accordance with research ethics board approval from the respective institutes. Informed consent was obtained from all patients included in this study. An overview of all samples included in different data collections is given in Figure S1A. All of the samples were independently reviewed by senior pediatric neuropathologists (S.A. and A.K.) according to the WHO guidelines. Detailed information about samples provided by TCGA can be found elsewhere (http://cancergenome.nih.gov).

DNA Methylation Profiling

For genome-wide assessment of DNA methylation GBM samples (n = 136) and controls (n = 10; four fetal and two adult samples of non-neoplastic cerebellum; two samples of Whole-Genome Amplified DNA (unmethylated control; two samples of M.SssI-treated DNA [100% methylated control]) were arrayed using the Illumina HumanMethylation450 BeadChip according to the manufacturer's instructions at the DKFZ. Methylation data of additional adult glioblastoma samples (n = 74) were obtained from the TCGA website (https://tcga-data.nci.nih.gov; available data from TCGA batches 79 and 111).

The following filtering criteria were applied: Removal of probes targeting the X and Y chromosomes (n = 11,551), removal of probes containing a single-nucleotide polymorphism (dbSNP132 Common) within five base pairs of and including the targeted CpG-site (n = 24,536), and probes not mapping uniquely to the human reference genome (hg19) allowing for one mismatch (n = 9,993). In total, 438,370 probes were kept for analysis.

For a subset of differentially methylated genes from the 450k array, MassARRAY technology (Sequenom, San Diego, CA, USA) was used to validate our results, allowing us to compare DNA methylation levels at 29 individual CpG-sites investigated by both techniques. DNA methylation measurements of those 29 CpG dinucleotides were highly correlated (median Pearson's correlation: r = 0.96; range: 0.71–1.00).

Gene Expression Profiling

Glioblastoma samples for which RNA of sufficient quantity and quality was available (n = 69) were analyzed on the Affymetrix GeneChip Human Genome U133 Plus 2.0 Array at the Microarray Department of the University of Amsterdam, the Netherlands. Sample library preparation, hybridization, and quality control were performed according to the manufacturer's protocols. Expression data were normalized using the MAS5.0 algorithm of the GCOS program (Affymetrix Inc). Gene expression data of additional adult glioblastoma samples (n = 74) were obtained from the TCGA website (https://tcga-data.nci.nih.gov; available data from TCGA batches 79 and 111). Predictive analysis of microarrays was used to assign TCGA methylation and gene expression subgroups to each of the samples in the present study.

Detection of CNAs

Copy-number aberrations were detected from the 450k Infinium methylation array in a custom approach using the sum of both methylated and unmethylated signals (Figure S1D). For the detection of *EGFR* and *PDGFRA* high-level amplifications, homozygous *CDKN2A* deletions, and CNAs affecting chromosomes 7 and 10 (as depicted in Figure 1), automatic scoring was verified by manual curation of the respective loci for each individual profile, and compared with results obtained from SNP profiling and fluorescence in situ hybridization (FISH) analysis where available. The three methodologies showed very high concordance.

Statistical Analysis and Measurement of Differential DNA Methylation and Gene Expression

For unsupervised consensus clustering we used the 8,000 most variable methylated probes (by standard deviation) across the data set (R package: clusterCons) (Monti et al., 2003; Wilkerson and Hayes, 2010). The consensus matrix was calculated using the k-means algorithm (10 random starting sets, maximum of 1,000 iterations) on a fraction of probes (0.8) in 1,000 iterations. The significance analysis of microarrays (SAM) method was used to identify genes that are differentially methylated or differentially expressed between subgroups. Correction for multiple testing was performed using the Benjamini-Hochberg method. Genes were considered significantly differentially methylated/expressed between two subgroups when displaying an adjusted p value < 0.01 and a methylation difference of 0.2 or a 2-fold change in expression.

Statistical Analysis of Clinical and Molecular Data

Kaplan-Meier analysis was performed to estimate the survival time of different GBM subgroups and a log rank test was used to test for differences of more than one survival curve. Comparisons of binary and categorical patient characteristics between subgroups were performed by the use of a two-sided Fisher's exact test. An unpaired t test was used to test for differences between the mean values for continuous variables in GBM subgroups.

Immunohistochemistry and FISH

Hematoxylin and eosin stained sections from all 143 paraffin blocks were prepared to define representative tumor regions for inclusion in the TMA. Antibodies against the following antigens were applied: OLIG2 (Millipore, Billerica, MA, USA; AB9610; dilution 1:250), FOXG1 (Abcam, Cambridge, UK; ab18259; dilution 1:50), ATRX (Sigma, HPA001906; dilution 1:750), and mutated IDH1 (R132H; (Capper et al., 2010; dianova, DIA H09). Multicolor interphase FISH analysis for *PDGFRA*, *EGFR,* and *CDKN2A* was performed as described (Pfister et al., 2009). Telomere-specific FISH was done using a standard formalin-fixed paraffin-embedded FISH protocol (Heaphy et al., 2011) using a FITC peptide nucleic acid telomere probe from Dako (Glostrup, Denmark).

Genomic Sequencing

Targeted sequencing of *H3F3A* (first coding exon), *IDH1* (exon 4), and *TP53* (all exons) was performed by QIAGEN (Hilden, Germany) in both forward and reverse directions using purified PCR products. PCR procedures were as previously described (Pfaff et al., 2010). Primer sequences are available upon request.

ACCESSION NUMBERS

The complete CpG methylation values have been deposited in NCBI's Gene Expression Omnibus (GEO; http://www.ncbi.nlm.nih.gov/geo) and are accessible through GEO Series accession number GSE36278. The complete gene expression values are accessible through GEO Series accession numbers GSE36245 and, as part of a previously reported series, GSE34824 (Schwartzentruber et al., 2012).

SUPPLEMENTAL INFORMATION

Supplemental Information includes five figures, four tables, and Supplemental Experimental Procedures and can be found with this article online at http://dx.doi.org/10.1016/j.ccr.2012.08.024.

ACKNOWLEDGMENTS

We thank Andrea Wittmann and Laura Sieber from the Division of Pediatric Neurooncology at the DKFZ for excellent technical support and Matthias Schick and Roger Fischer from the DKFZ Genomics and Proteomics Core Facility for performing the microarray analyses to a very high standard. We also acknowledge the outstanding technical assistance of Hannelore Schraut (University of Würzburg) and Leonore Senf (Nürnberg Children's Hospital). The project was supported by grants from the German Cancer Aid (109252 and 108456); the BMBF (to A.K., B.R., O.W., P.L., S.M.P., G.R., and J.F.; ICGC PedBrain, NGFN^{Plus} #01GS0883); Koningin Wilhelmina Fonds (UvA-2010-4713) and KIKA (to M.K.); the Cole Foundation; the Canadian Institute of Health Research; the Institute of Cancer Research, Génome Canada and Génome Quebec (to N.J.); and the Alfred-Müller Award for Neuro-Oncology to S.M.P.

Received: February 22, 2012
Revised: June 3, 2012
Accepted: August 24, 2012
Published: October 15, 2012

REFERENCES

Antonelli, M., Buttarelli, F.R., Arcella, A., Nobusawa, S., Donofrio, V., Oghaki, H., and Giangaspero, F. (2010). Prognostic significance of histological grading, p53 status, *YKL-40* expression, and *IDH1* mutations in pediatric high-grade gliomas. J. Neurooncol. *99*, 209–215.

Balss, J., Meyer, J., Mueller, W., Korshunov, A., Hartmann, C., and von Deimling, A. (2008). Analysis of the *IDH1* codon 132 mutation in brain tumors. Acta Neuropathol. *116*, 597–602.

Bax, D.A., Mackay, A., Little, S.E., Carvalho, D., Viana-Pereira, M., Tamber, N., Grigoriadis, A.E., Ashworth, A., Reis, R.M., Ellison, D.W., et al. (2010). A distinct spectrum of copy number aberrations in pediatric high-grade gliomas. Clin. Cancer Res. *16*, 3368–3377.

Brinkman, A.B., Gu, H., Bartels, S.J., Zhang, Y., Matarese, F., Simmer, F., Marks, H., Bock, C., Gnirke, A., Meissner, A., and Stunnenberg, H.G. (2012). Sequential ChIP-bisulfite sequencing enables direct genome-scale investigation of chromatin and DNA methylation cross-talk. Genome Res. *22*, 1128–1138.

Broniscer, A., Baker, S.J., West, A.N., Fraser, M.M., Proko, E., Kocak, M., Dalton, J., Zambetti, G.P., Ellison, D.W., Kun, L.E., et al. (2007). Clinical and molecular characteristics of malignant transformation of low-grade glioma in children. J. Clin. Oncol. *25*, 682–689.

Capper, D., Weissert, S., Balss, J., Habel, A., Meyer, J., Jäger, D., Ackermann, U., Tessmer, C., Korshunov, A., Zentgraf, H., et al. (2010). Characterization of R132H mutation-specific IDH1 antibody binding in brain tumors. Brain Pathol. *20*, 245–254.

Chowdhury, R., Yeoh, K.K., Tian, Y.M., Hillringhaus, L., Bagg, E.A., Rose, N.R., Leung, I.K., Li, X.S., Woon, E.C., Yang, M., et al. (2011). The oncometabolite 2-hydroxyglutarate inhibits histone lysine demethylases. EMBO Rep. *12*, 463–469.

Christensen, B.C., Smith, A.A., Zheng, S., Koestler, D.C., Houseman, E.A., Marsit, C.J., Wiemels, J.L., Nelson, H.H., Karagas, M.R., Wrensch, M.R., et al. (2011). DNA methylation, isocitrate dehydrogenase mutation, and survival in glioma. J. Natl. Cancer Inst. *103*, 143–153.

Dang, L., White, D.W., Gross, S., Bennett, B.D., Bittinger, M.A., Driggers, E.M., Fantin, V.R., Jang, H.G., Jin, S., Keenan, M.C., et al. (2009). Cancer-associated IDH1 mutations produce 2-hydroxyglutarate. Nature *462*, 739–744.

De Carli, E., Wang, X., and Puget, S. (2009). IDH1 and IDH2 mutations in gliomas. N. Engl. J. Med. *360*, 2248.

Drané, P., Ouararhni, K., Depaux, A., Shuaib, M., and Hamiche, A. (2010). The death-associated protein DAXX is a novel histone chaperone involved in the replication-independent deposition of H3.3. Genes Dev. *24*, 1253–1265.

Gibbons, R.J., McDowell, T.L., Raman, S., O'Rourke, D.M., Garrick, D., Ayyub, H., and Higgs, D.R. (2000). Mutations in ATRX, encoding a SWI/SNF-like protein, cause diverse changes in the pattern of DNA methylation. Nat. Genet. *24*, 368–371.

Goldberg, A.D., Banaszynski, L.A., Noh, K.M., Lewis, P.W., Elsaesser, S.J., Stadler, S., Dewell, S., Law, M., Guo, X., Li, X., et al. (2010). Distinct factors control histone variant H3.3 localization at specific genomic regions. Cell *140*, 678–691.

Gonzalo, S., Jaco, I., Fraga, M.F., Chen, T., Li, E., Esteller, M., and Blasco, M.A. (2006). DNA methyltransferases control telomere length and telomere recombination in mammalian cells. Nat. Cell Biol. *8*, 416–424.

Heaphy, C.M., de Wilde, R.F., Jiao, Y., Klein, A.P., Edil, B.H., Shi, C., Bettegowda, C., Rodriguez, F.J., Eberhart, C.G., Hebbar, S., et al. (2011). Altered telomeres in tumors with ATRX and DAXX mutations. Science *333*, 425.

Hyland, E.M., Molina, H., Poorey, K., Jie, C., Xie, Z., Dai, J., Qian, J., Bekiranov, S., Auble, D.T., Pandey, A., and Boeke, J.D. (2011). An evolutionarily 'young' lysine residue in histone H3 attenuates transcriptional output in Saccharomyces cerevisiae. Genes Dev. *25*, 1306–1319.

Kaneda, A., Kaminishi, M., Yanagihara, K., Sugimura, T., and Ushijima, T. (2002). Identification of silencing of nine genes in human gastric cancers. Cancer Res. *62*, 6645–6650.

Kang, H.J., Kawasawa, Y.I., Cheng, F., Zhu, Y., Xu, X., Li, M., Sousa, A.M., Pletikos, M., Meyer, K.A., Sedmak, G., et al. (2011). Spatio-temporal transcriptome of the human brain. Nature *478*, 483–489.

Khuong-Quang, D.A., Buczkowicz, P., Rakopoulos, P., Liu, X.Y., Fontebasso, A.M., Bouffet, E., Bartels, U., Albrecht, S., Schwartzentruber, J., Letourneau, L., et al. (2012). K27M mutation in histone H3.3 defines clinically and biologically distinct subgroups of pediatric diffuse intrinsic pontine gliomas. Acta Neuropathol. *124*, 439–447.

Ligon, K.L., Alberta, J.A., Kho, A.T., Weiss, J., Kwaan, M.R., Nutt, C.L., Louis, D.N., Stiles, C.D., and Rowitch, D.H. (2004). The oligodendroglial lineage marker OLIG2 is universally expressed in diffuse gliomas. J. Neuropathol. Exp. Neurol. *63*, 499–509.

Louis, D.N., Ohgaki, H., Wiestler, O.D., and Cavenee, W.K. (2007). WHO Classification of Tumors of the Central Nervous System (Lyon: IARC).

Lu, C., Ward, P.S., Kapoor, G.S., Rohle, D., Turcan, S., Abdel-Wahab, O., Edwards, C.R., Khanin, R., Figueroa, M.E., Melnick, A., et al. (2012). IDH mutation impairs histone demethylation and results in a block to cell differentiation. Nature *483*, 474–478.

McLendon, R., Friedman, A., Bigner, D., Van Meir, E.G., Brat, D.J., Mastrogianakis, M., Olson, J.J., Mikkelsen, T., Lehman, N., Aldape, K., et al; Cancer Genome Atlas Research Network. (2008). Comprehensive genomic characterization defines human glioblastoma genes and core pathways. Nature *455*, 1061–1068.

Mehta, S., Huillard, E., Kesari, S., Maire, C.L., Golebiowski, D., Harrington, E.P., Alberta, J.A., Kane, M.F., Theisen, M., Ligon, K.L., et al. (2011). The central nervous system-restricted transcription factor Olig2 opposes p53 responses to genotoxic damage in neural progenitors and malignant glioma. Cancer Cell *19*, 359–371.

Meissner, A., Mikkelsen, T.S., Gu, H., Wernig, M., Hanna, J., Sivachenko, A., Zhang, X., Bernstein, B.E., Nusbaum, C., Jaffe, D.B., et al. (2008). Genome-scale DNA methylation maps of pluripotent and differentiated cells. Nature *454*, 766–770.

Monti, S., Tamayo, P., Mesirov, J., and Golub, T. (2003). Consensus clustering: A resampling-based method for class discovery and visualization of gene expression microarray data. Mach. Learn. *52*, 91–118.

Noushmehr, H., Weisenberger, D.J., Diefes, K., Phillips, H.S., Pujara, K., Berman, B.P., Pan, F., Pelloski, C.E., Sulman, E.P., Bhat, K.P., et al; Cancer Genome Atlas Research Network. (2010). Identification of a CpG island methylator phenotype that defines a distinct subgroup of glioma. Cancer Cell *17*, 510–522.

Pang, J.C., Li, K.K., Lau, K.M., Ng, Y.L., Wong, J., Chung, N.Y., Li, H.M., Chui, Y.L., Lui, V.W., Chen, Z.P., et al. (2010). *KIAA0495/PDAM* is frequently down-regulated in oligodendroglial tumors and its knockdown by siRNA induces cisplatin resistance in glioma cells. Brain Pathol. *20*, 1021–1032.

Parsons, D.W., Jones, S., Zhang, X., Lin, J.C., Leary, R.J., Angenendt, P., Mankoo, P., Carter, H., Siu, I.M., Gallia, G.L., et al. (2008). An integrated genomic analysis of human glioblastoma multiforme. Science *321*, 1807–1812.

Paugh, B.S., Qu, C., Jones, C., Liu, Z., Adamowicz-Brice, M., Zhang, J., Bax, D.A., Coyle, B., Barrow, J., Hargrave, D., et al. (2010). Integrated molecular genetic profiling of pediatric high-grade gliomas reveals key differences with the adult disease. J. Clin. Oncol. *28*, 3061–3068.

Paugh, B.S., Broniscer, A., Qu, C., Miller, C.P., Zhang, J., Tatevossian, R.G., Olson, J.M., Geyer, J.R., Chi, S.N., da Silva, N.S., et al. (2011). Genome-wide analyses identify recurrent amplifications of receptor tyrosine kinases and cell-cycle regulatory genes in diffuse intrinsic pontine glioma. J. Clin. Oncol. *29*, 3999–4006.

Pfaff, E., Remke, M., Sturm, D., Benner, A., Witt, H., Milde, T., von Bueren, A.O., Wittmann, A., Schöttler, A., Jorch, N., et al. (2010). *TP53* mutation is frequently associated with *CTNNB1* mutation or *MYCN* amplification and is compatible with long-term survival in medulloblastoma. J. Clin. Oncol. *28*, 5188–5196.

Pfister, S., Remke, M., Benner, A., Mendrzyk, F., Toedt, G., Felsberg, J., Wittmann, A., Devens, F., Gerber, N.U., Joos, S., et al. (2009). Outcome prediction in pediatric medulloblastoma based on DNA copy-number aberrations of chromosomes 6q and 17q and the *MYC* and *MYCN* loci. J. Clin. Oncol. *27*, 1627–1636.

Pollack, I.F., Hamilton, R.L., Sobol, R.W., Nikiforova, M.N., Lyons-Weiler, M.A., Laframboise, W.A., Burger, P.C., Brat, D.J., Rosenblum, M.K., Holmes, E.J., et al. (2011). IDH1 mutations are common in malignant gliomas arising in adolescents: A report from the Children's Oncology Group. Childs Nerv. Syst. *27*, 87–94. Published online August 20, 2010. http://dx.doi.org/10.1007/s00381-010-1264-1.

Puget, S., Philippe, C., Bax, D.A., Job, B., Varlet, P., Junier, M.P., Andreiuolo, F., Carvalho, D., Reis, R., Guerrini-Rousseau, L., et al. (2012). Mesenchymal transition and *PDGFRA* amplification/mutation are key distinct oncogenic events in pediatric diffuse intrinsic pontine gliomas. PLoS ONE *7*, e30313.

Qu, H.Q., Jacob, K., Fatet, S., Ge, B., Barnett, D., Delattre, O., Faury, D., Montpetit, A., Solomon, L., Hauser, P., et al. (2010). Genome-wide profiling using single-nucleotide polymorphism arrays identifies novel chromosomal imbalances in pediatric glioblastomas. Neuro-oncol. *12*, 153–163.

Schiffman, J.D., Hodgson, J.G., VandenBerg, S.R., Flaherty, P., Polley, M.Y., Yu, M., Fisher, P.G., Rowitch, D.H., Ford, J.M., Berger, M.S., et al. (2010). Oncogenic BRAF mutation with CDKN2A inactivation is characteristic of a subset of pediatric malignant astrocytomas. Cancer Res. *70*, 512–519.

Schwartzentruber, J., Korshunov, A., Liu, X.Y., Jones, D.T.W., Pfaff, E., Jacob, K., Sturm, D., Fontebasso, A.M., Quang, D.A., Tönjes, M., et al. (2012). Driver mutations in histone H3.3 and chromatin remodelling genes in paediatric glioblastoma. Nature *482*, 226–231.

Setty, P., Hammes, J., Rothämel, T., Vladimirova, V., Kramm, C.M., Pietsch, T., and Waha, A. (2010). A pyrosequencing-based assay for the rapid detection of *IDH1* mutations in clinical samples. J. Mol. Diagn. *12*, 750–756.

Statham, A.L., Robinson, M.D., Song, J.Z., Coolen, M.W., Stirzaker, C., and Clark, S.J. (2012). Bisulfite sequencing of chromatin immunoprecipitated DNA (BisChIP-seq) directly informs methylation status of histone-modified DNA. Genome Res. *22*, 1120–1127.

Turcan, S., Rohle, D., Goenka, A., Walsh, L.A., Fang, F., Yilmaz, E., Campos, C., Fabius, A.W., Lu, C., Ward, P.S., et al. (2012). IDH1 mutation is sufficient to establish the glioma hypermethylator phenotype. Nature *483*, 479–483.

Verhaak, R.G., Hoadley, K.A., Purdom, E., Wang, V., Qi, Y., Wilkerson, M.D., Miller, C.R., Ding, L., Golub, T., Mesirov, J.P., et al; Cancer Genome Atlas Research Network. (2010). Integrated genomic analysis identifies clinically relevant subtypes of glioblastoma characterized by abnormalities in *PDGFRA, IDH1, EGFR*, and *NF1*. Cancer Cell *17*, 98–110.

Wang, Y., Yang, J., Zheng, H., Tomasek, G.J., Zhang, P., McKeever, P.E., Lee, E.Y., and Zhu, Y. (2009). Expression of mutant p53 proteins implicates a lineage relationship between neural stem cells and malignant astrocytic glioma in a murine model. Cancer Cell *15*, 514–526.

Wilkerson, M.D., and Hayes, D.N. (2010). ConsensusClusterPlus: a class discovery tool with confidence assessments and item tracking. Bioinformatics *26*, 1572–1573.

Wu, G., Broniscer, A., McEachron, T.A., Lu, C., Paugh, B.S., Becksfort, J., Qu, C., Ding, L., Huether, R., Parker, M., et al; St. Jude Children's Research Hospital–Washington University Pediatric Cancer Genome Project. (2012). Somatic histone H3 alterations in pediatric diffuse intrinsic pontine gliomas and non-brainstem glioblastomas. Nat. Genet. *44*, 251–253.

Xu, W., Yang, H., Liu, Y., Yang, Y., Wang, P., Kim, S.H., Ito, S., Yang, C., Wang, P., Xiao, M.T., et al. (2011). Oncometabolite 2-hydroxyglutarate is a competitive inhibitor of α-ketoglutarate-dependent dioxygenases. Cancer Cell *19*, 17–30.

Yan, H., Parsons, D.W., Jin, G., McLendon, R., Rasheed, B.A., Yuan, W., Kos, I., Batinic-Haberle, I., Jones, S., Riggins, G.J., et al. (2009). IDH1 and IDH2 mutations in gliomas. N. Engl. J. Med. *360*, 765–773.

Zarghooni, M., Bartels, U., Lee, E., Buczkowicz, P., Morrison, A., Huang, A., Bouffet, E., and Hawkins, C. (2010). Whole-genome profiling of pediatric diffuse intrinsic pontine gliomas highlights platelet-derived growth factor receptor alpha and poly (ADP-ribose) polymerase as potential therapeutic targets. J. Clin. Oncol. *28*, 1337–1344.